High resolution stimulated resonant Raman spectroscopy of I_2 in the $X^1\Sigma_{0^+g}(v=0, J=13)$ state.

A. N. Goncharov
Institute of Laser Physics, Siberian branch of Russian Academy of Sciences

F. Du Burck, N. Courtier, M. Gorlicki, G. Camy and Ch. J. Bordé
Laboratoire de Physique des Lasers, Université Paris-Nord

1. INTRODUCTION

Stimulated resonant Raman (SRR) processes have been widely used for high precision spectroscopy of atoms and molecules [1], especially when the levels of interest are metastable. Owing to the long lifetime of these levels, one may obtain extremely narrow SRR resonances which are useful both for spectroscopic and metrological applications [2]. There is a close analogy between the SRR interaction of the three-level system with two laser beams at frequencies ν_1, ν_2, and the interaction of the two ground level hyperfine states with a microwave radiation at the frequency $(\nu_1 - \nu_2)$. Because of this analogy, our experiment has some common features with that of optical microwave double resonance [3], but it provides a better signal-to-noise ratio and a simpler experimental set-up. The present paper illustrates how useful SRR spectroscopy can be for the study of hyperfine structure of the ground electronic state of I_2.

We have indeed observed SRR transitions between hyperfine sublevels of the ground electronic state $X^1\Sigma_{0^+g}(v=0, J=13)$ of I_2 and resonances narrower than 10 kHz (HWHM) have been obtained. We have measured six hyperfine transitions with a 0.2 kHz accuracy. A pressure broadening of the SRR transitions equal to 7 ± 1 kHz/mtorr has been found. A third-order calculation of the line shape based on the diagrammatic representation of the density matrix equations is presented. The experimental line shapes of the SRR resonances are in good qualitative agreement with the results of the calculation. The advantages of this method for high precision spectroscopy of iodine are discussed.

2. EXPERIMENT AND RESULTS

Figure 1(a) shows the diagram of hyperfine sublevels between which a SRR transition is induced by two laser waves at frequencies ν_1 and ν_2. The sublevels of interest are the same as in the case of crossover resonances with a common upper level (b) [4].

The experimental setup is shown in figure 2. The laser beam at the frequency ν_2 is provided by a monomode prestabilised Ar^+ laser [5]. The beam at the frequency ν_1 is generated from the previous one by means of two acoutooptic modulators (AOM). In order to reduce the beams misalignment coming from frequency modulation and frequency scanning of ν_1, AOM2 is used in a double-pass geometry. AOM1 provides the optical isolation of the laser from back-scattering and increases the range of available detunings. The perpendicularly polarized beams at the frequencies ν_1 and ν_2 are combined in a Glan prism. To reduce the errors induced by the relative misalignment of the laser beams and to decrease the transit-broadening of resonances, an expansion of the laser beams up to a diameter $2w_0 \approx 1$ cm is used. First-derivative resonance signals are obtained by FM modulation ($f_{mod} = 5$ kHz) of AOM2 generator followed by phase sensitive detection of the laser beam at the frequency ν_2. Figure 1(b) shows a typical signal corresponding to the SRR transition between the hyperfine sublevels ($\varepsilon' = 5$, $F' = 10$) and ($\varepsilon'' = 5$, $F'' = 9$). The recording was made under the conditions which we usually used for the line center measurements : the I_2 pressure was 2

mtorr ; the average power densities of the laser beams in the cell were 5 mW/cm^2 and 10 mW/cm^2 at frequencies ν_1 and ν_2 respectively ; the amplitude and the frequency of the probe modulation were 10 kHz and 5 kHz respectively.

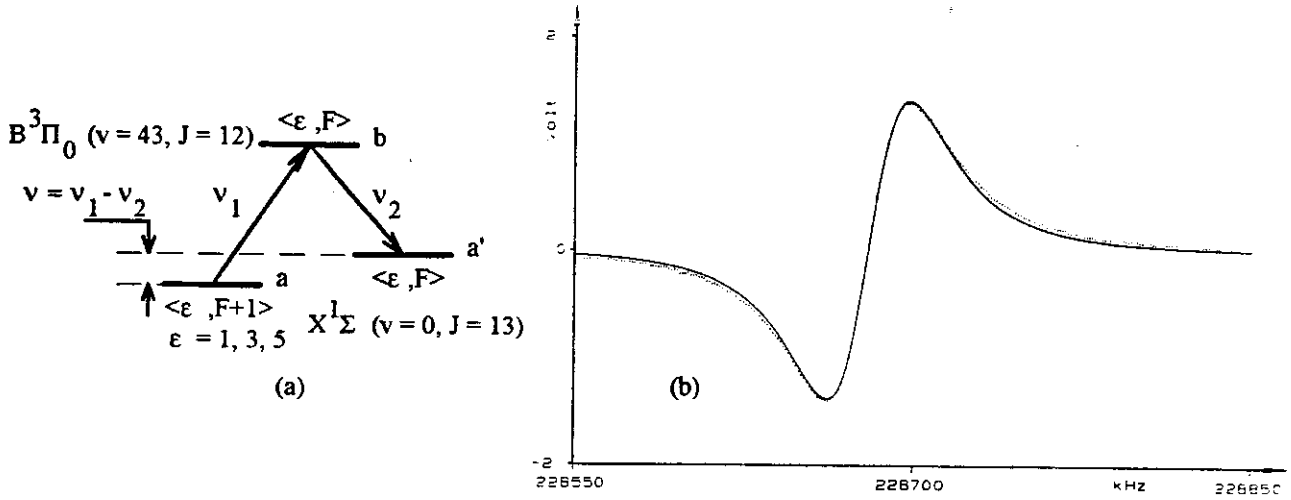

Fig. 1. (a) Schematic representation of the SRR interaction process involving hyperfine sublevels of the X(v = 0, J = 13) state in iodine ; (b) SRR resonance between hyperfine sublevels (ε′ = 5, F′ = 10) and (ε″ = 5, F″ = 9). The lock-in amplifier time constant was 0.1s. The solid line is the first-derivative of a pure Lorentzian with half-width 30 kHz.

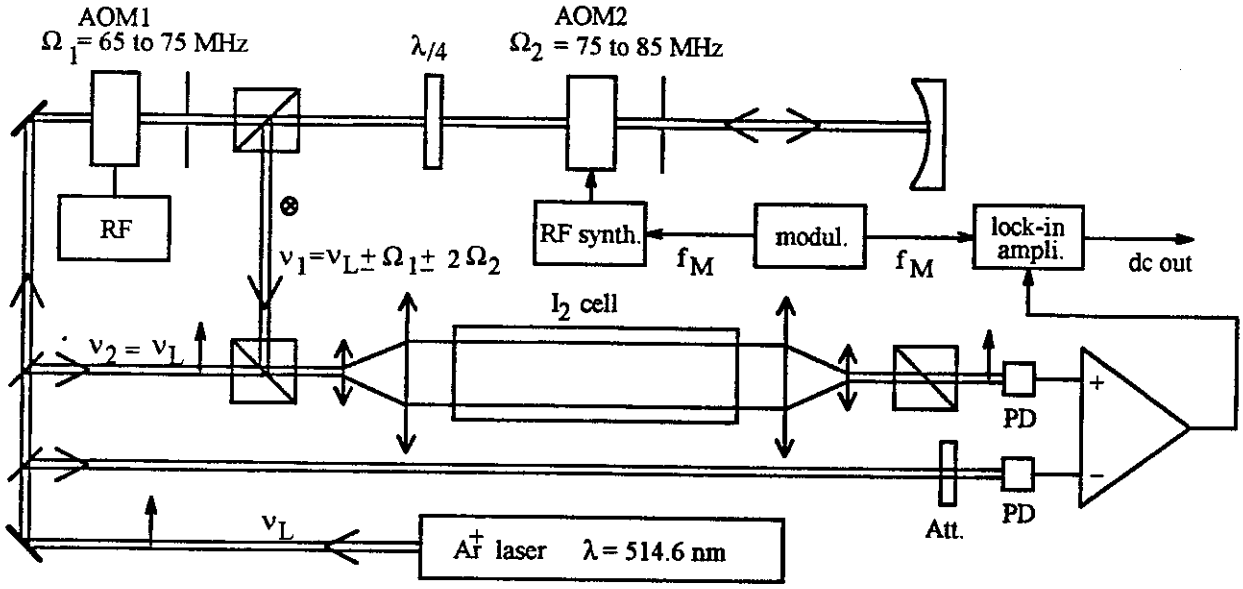

Fig. 2. Schematic representation of the experimental set-up.

To measure the pressure broadening of the SRR resonances, the pressure of I_2 was increased from 0.4 mtorr to 70 mtorr and the resonance shapes were fitted by Lorentzian derivatives whose widths were extrapolated to zero power intensity and zero amplitude of the probe modulation. Figure 3 presents the resonance halfwidth $\gamma_{aa'}/2\pi$ versus the pressure of I_2. We have found a linear dependence of $\gamma_{aa'}/2\pi$ with the iodine pressure. The slope coefficient is equal to :

$$\frac{1}{2\pi}\frac{d\gamma_{aa'}}{dP} = 7 \pm 1 \text{ kHz / mtorr.}$$

This result when compared with those obtained in ref. [6] may provide information on the dephasing collisions of iodine molecules. The half-width of the narrowest resonance obtained was $\gamma_{aa'}/2\pi \equiv 8$ kHz under the following conditions : iodine pressure 0.3 mtorr ; amplitude of the probe modulation 3 kHz ; power density in the cell $I \leq 2 \text{mW/cm}^2$. This value may be explained by a residual misalignment of the laser beams and by a transit broadening.

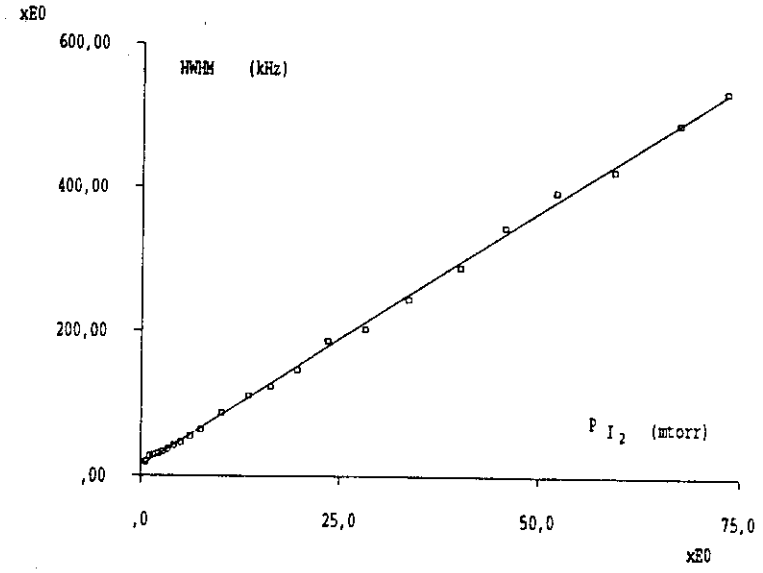

Fig. 3. Half-width of the SRR resonance fitted by a Lorentzian derivative versus iodine pressure in the cell. The solid line represents $\gamma_{aa'}/2\pi = 13.6 \text{ kHz} + 7.08 \text{ kHz/mtorr} * P_{I_2}$ (result of the linear regression). The experimental values of the resonance halfwidths at pressures greater than 40 mtorr were obtained without telescope.

According to the possibilites of our AOMs, the measurements of six SRR transitions could be made. Table 1 presents our results and the results of ref. [3]. The agreement between them, better than 1 kHz, illustrates the accuracy of our measurements. Within the accuracy of our experiment, we have not found any pressure shift of the SRR resonances.

TABLE 1 . SRR transitions between hyperfine sublevels in the state $X(v = 0, J = 13)$ of I_2.

$\varepsilon', F' \rightarrow \varepsilon'', F''$	Result of ref. [3] (kHz)[a]	Our results (kHz)[a]
5,13 → 5,14	---------	75378.4(2)
5,11 → 5,12	---------	87250.1(2)
5,15 → 5,14	100892.7(4)	100893.5(2)
3,15 → 3,14	212479.3(4)	212479.1(2)
5,13 → 5,12	218699.0(4)	218699.2(2)
5,10 → 5,9	228679.1(1)	228679.3(2)

[a] Numbers in parentheses are estimates of experimental reproducibilities in units of 0.1 kHz

To illustrate the small influence of the beams divergence, the line shape of the SRR resonances have been recorded with a beam expander out of focus. Figure 4 presents the line shape of the SRR resonances with a beam divergence angle θ equal to 0.43°, 0° and -0.5° respectively. The I_2 pressure in the cell was 0.3 mtorr. The solid line (Fig.4) is the result of the line shape calculations under the following conditions :

$$(\gamma_{ab}, \gamma_{a'b})/2\pi \cong 100 \text{ kHz}, \quad \gamma_{aa'}/2\pi \cong 10 \text{ kHz}, \quad w_0 = \lambda/\pi\theta = 2\cdot10^{-3} \text{ cm}, \quad w = 0.5 \text{ cm}.$$

The calculated line shape, as well as the experimental one, show a large asymmetry but only a small broadening (the usual saturated absorption resonance broadening under these conditions is equal to 2.5 MHz).

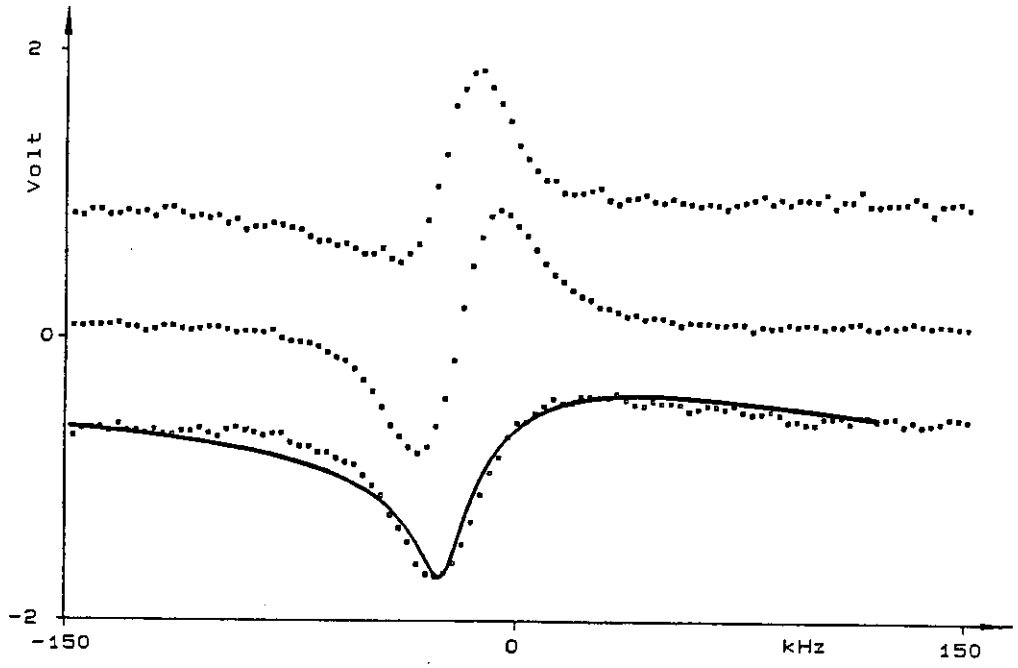

Fig. 4. Line shape of the SRR resonances with a beam divergence angle θ equal respectively to 0.43°, 0°, -0.5° from top to bottom ; the solid line is the result of the line shape calculation under the following conditions :
$(\gamma_{ab}, \gamma_{a'b})/2\pi \cong 100$ kHz, $\gamma_{aa'}/2\pi \cong 10$ kHz, $w_0 = \lambda/\pi\theta = 2\cdot10^{-3}$ cm, $w = 0.5$ cm.

3. LINE SHAPE CALCULATION

This line shape is derived using the diagrammatic representation of the density matrix equations described in [7] and it follows closely earlier derivations of the Doppler-free two-photon line shape [8] and of the saturated absorption line shape [9]. This technique provides a set of computation rules associated with a time-ordered double Feynman diagram representing a given process. In addition to the relaxation mechanisms ($\gamma_{\alpha\beta}$), velocity-changing collisions, light shifts, polarization and frequency modulation of the laser beams, molecular phase space distribution $F(x,y,z,v_x,v_y,v_z)$, it includes all effects resulting from the molecular motion :
-transit effects through the beam geometry U(x,y,z) including beam curvature,
-first and second-order Doppler effects,
-recoil shifts ($\delta = hk^2/4\pi M$).

Figure 5 presents the time-ordered double Feynman diagram for our SRR process.

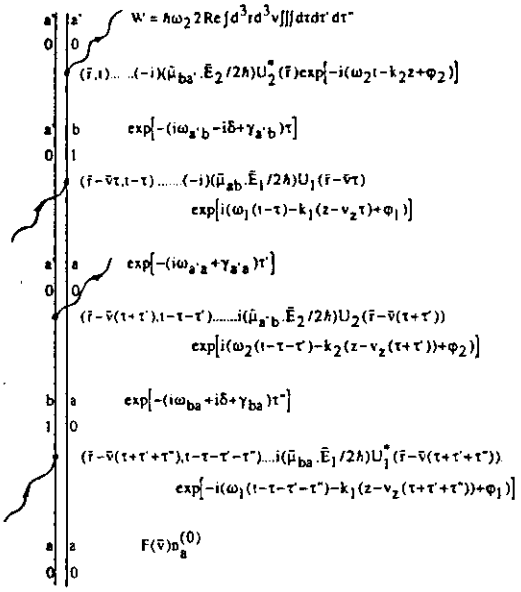

Fig. 5. Time-ordered double Feynman diagram (density matrix diagram) for the SRR process.

As a final result of the diagrammatic calculation, the SRR power absorbed per unit length for the laser beam with the frequency ν_2 is found to be :

$$\frac{dW}{dz} = n_a^{(0)} \Pi_\Omega \hbar\omega_2 \frac{2\sqrt{\pi}}{ku} \alpha(z) S(\Delta),$$

where $\Pi_\Omega = \frac{\vec{\mu}_{ba'} \cdot \vec{E}_2}{2\hbar} \frac{\vec{\mu}_{ab} \cdot \vec{E}_1}{2\hbar} \frac{\vec{\mu}_{a'b} \cdot \vec{E}_2}{2\hbar} \frac{\vec{\mu}_{ba} \cdot \vec{E}_1}{2\hbar}$. $S(\Delta)$ gives the lineshape :

$$S(\Delta) = \mathrm{Re} \int_0^{+\infty} d\tau \int_0^{+\infty} d\tau' \frac{\exp\left[\left(i\Delta - 2\gamma_{ba}\right)\tau\right] \exp\left[\left(i\Delta - \gamma_{aa'}\right)\tau'\right]}{1 + Au^2\tau'^2 + 2Bu^2\tau\tau' + Cu^2\tau^2} =$$

$$= \mathrm{Im}\left\{ \frac{\gamma_{aa'} - i\Delta}{2Au^2} \int_0^{+\infty} d\tau \frac{e^{Z_2} E_1(Z_2) - e^{Z_1} E_1(Z_1)}{Y} e^{\left(i\Delta - 2\gamma_{ba}\right)\tau} \right\},$$

where E_1 is the exponential integral function, with :

$$Z_{1,2} = X \pm iY = (\gamma_{aa'} - i\Delta)\left[\frac{B}{A}\tau \pm \frac{i}{u\sqrt{A}} (1 + Du^2\tau^2)^{1/2} \right] \; ; \; \Delta = \omega_1 - \omega_2 - \omega_{aa'} \; ; \; u = \sqrt{\frac{2kT}{M}},$$

where the coefficients A, B, C, D and $\alpha(z)$ depend only upon the beam geometry. For matched beams with a common waist of radius w_0 and confocal parameter $b = kw_0^2$:

$$A = \frac{1}{w^2(z)} \; ; \; B = l^* \; ; \; C = 2l^* \; ; \; D = C - \frac{B^2}{A} = \frac{1}{w_0^2} \; ;$$

$$l = \frac{L}{w_0^2} \; ; \; L = \frac{1}{1 - 2iz/b} \; ; \; \alpha(z) = \left(\frac{1}{1 + (2z/b)^2} \right)^2 \frac{\pi w^2(z)}{2}.$$

Figure 6(a) shows the result of the line shape calculation in the transit time limit. Figure 6(b) presents result of the line shape calculation under conditions close to our experimental situation.

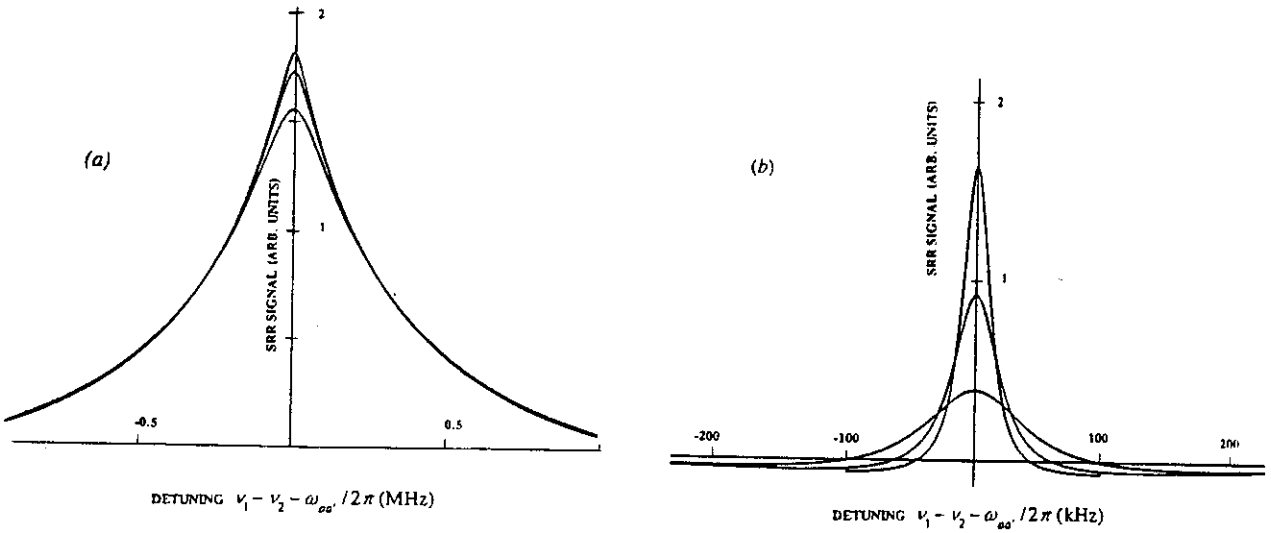

Fig. 6. (a) Results of the line shape calculations in the transit-time limit : $u/2\pi w_0 \approx 1$MHz ($w_0 = 2\cdot 10^{-3}$ cm), $\gamma_{ab}/2\pi = 100$ kHz, $\gamma_{aa'}/2\pi$ equal to 10, 20 and 50 kHz ; (b) Results of the line shape calculations under the following conditions $u/2\pi w_0 \approx 4.5$ kHz ($w_0 = 0.5$ cm), $\gamma_{ab}/2\pi = 100$ kHz, $\gamma_{aa'}/2\pi$ equal to 10, 20 and 50 kHz

If $\gamma_{ba} >> \gamma_{aa'}$ and $z << b$ the previous integrals simplify to :

$$S(\Delta) = \frac{1}{2u\sqrt{A}} \frac{1}{2\gamma_{ab}} \mathrm{Im}\left\{ E_1\left(-\frac{i\gamma_{aa'}+\Delta}{u\sqrt{A}}\right)\exp\left(-\frac{i\gamma_{aa'}+\Delta}{u\sqrt{A}}\right) - E_1\left(\frac{i\gamma_{aa'}+\Delta}{u\sqrt{A}}\right)\exp\left(\frac{i\gamma_{aa'}+\Delta}{u\sqrt{A}}\right)\right\}$$

which goes into a double exponential in the pure transit limit :

$$S(\Delta) = \frac{\pi}{2u\sqrt{A}} \frac{1}{2\gamma_{ab}} \exp\left(-\frac{|\Delta|}{u\sqrt{A}}\right),$$

and into a Lorentzian of width $\gamma_{aa'}$ in the high pressure limit :

$$S(\Delta) = \frac{1}{2\gamma_{ab}\,\gamma_{a'a}} \frac{\gamma_{aa'}^2}{\gamma_{aa'}^2 + \Delta^2}.$$

Figure 7 represents the dependence of the peak-to-peak width of the SRR resonance versus $\gamma_{aa'}$.

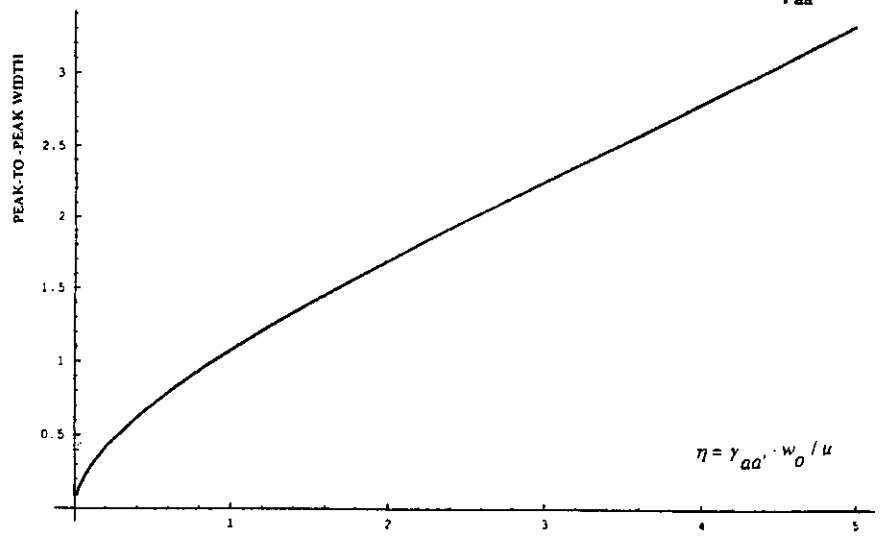

Fig. 7. Peak to peak width of the calculated line shape derivative as a function of $\eta = \gamma_{aa'} w_0 / u$. For the large values of $\gamma_{aa'}$, this curve goes asymptoticaly to a straight line the slope of which is $1/\sqrt{3}$; for the small values of $\gamma_{aa'}$, it is given by $2\times(2\eta/\pi)^{1/2}$.

4. SUMMARY

As a conclusion, the experimental method presented here, gives the possibility of accurate and independent measurements of the lower level hyperfine structure of molecules. As it was shown in refs. [3,5], independent measurements of the hyperfine interaction constants of the lower level, together with the measurement of the hyperfine structure of the $X \rightarrow B$ transitions, improve the accuracy of the fitting procedure, which is used to evaluate the constants of hyperfine interactions.

The results of the line shape calculations explain the main features of the SRR resonances. When $\gamma_{aa'} << \gamma_{ab}, \gamma_{a'b}$, the line shape differs from a Lorentzian. In the transit-time broadening limit, (i.e. when $u/w \geq \gamma_{aa'}$), the SRR resonance exhibits a double exponential line shape with a sharp top. As in the case of saturated absorption, this phenomenon may be explained by a "velocity selection" effect [9]. As far as only the divergence of the laser beam is concerned, the behaviour of the SRR resonances differs strongly from the case of saturated absorption. The SRR resonances probe the local size of the laser beam and are relatively insensitive to the beam divergence, or to wave front distortions by cell windows. So, with a beam diameter of the order 1-2 cm in a low pressure I_2 cell, one may obtain sub-kilohertz SRR resonances useful both for high precision spectroscopy and for metrology.

5. ACKNOWLEDGMENTS

One of us (A. N. G.) thanks the Laboratoire de Physique des Lasers for hospitality and the Ministère de l'Enseignement Supérieur et de la Recherche for research grant.

6. REFERENCES

1. I. M. Beterov and V. P. Chebotayev, in Progress in Quantum Electronics, edited by John H. Sanders et al. (Pergamon, Oxford, England, 1974) vol.3, Pt.1, and references therein ; P. R. Hemmer, M. S. Shahriar, V. D. Natoli, and S. Ezekiel, J. Opt. Soc. Am. B6, 1519 (1989), and references therein.
2. P. R. Hemmer and S. Ezekiel,C. C. Leiby, Jr.,Opt. Lett. 8, 440 (1983).
3. A. Yokozeki and J. S. Muenter, J. Chem. Phys. 72(6), 3796 (1980).
4. Ch. J. Bordé, G. Camy, B. Decomps, Phys. Rev. A20, 254 (1979).
5. Ch. J. Bordé, G. Camy, J.P. Descoubes, J. Vigue, J. Physique 42, 1393 (1981).
6. A. N. Goncharov, M. N. Skvortsov and V. P. Chebotayev, Appl. Phys. B51, 108 (1990).
7. Ch. J. Bordé, in Advances in Laser Spectroscopy, edited by F. T. Arecchi, F. Strumia, and H. Walther (Plenum Publishing Corporation, 1983).
8. Ch. J. Bordé, C.R.Acad.Sc. Paris 282B, 341 (1976).
9. Ch. J. Bordé, J. L. Hall, C. V. Kunasz, and D. G. Hummer, Phys. Rev. A14, 236 (1976).